crystals

MDPI

Review

Recent Progress in True 3D Display Technologies Based on Liquid Crystal Devices

Shuxin Liu *, Yan Li and Yikai Su *

Department of Electronic Engineering, Shanghai Jiao Tong University, Shanghai 200240, China
* Correspondence: liushuxin@sjtu.edu.cn (S.L.); yikaisu@sjtu.edu.cn (Y.S.)

Abstract: In recent years, the emergence of virtual reality (VR) and augmented reality (AR) has revolutionized the way we interact with the world, leading to significant advancements in 3D display technology. However, some of the currently employed 3D display techniques rely on stereoscopic 3D display method, which may lead to visual discomfort due to the vergence-accommodation conflict. To address this issue, several true 3D technologies have been proposed as alternatives, including multi-plane displays, holographic displays, super multi-view displays, and integrated imaging displays. In this review, we focus on planar liquid crystal (LC) devices for different types of true 3D display applications. Given the excellent optical performance of the LC devices, we believe that LC devices hold great potential for true 3D displays.

Keywords: 3D display; liquid crystal devices; AR/VR display; Pancharatnam–Berry phase

Citation: Liu, S.; Li, Y.; Su, Y. Recent Progress in True 3D Display Technologies Based on Liquid Crystal Devices. *Crystals* **2023**, *13*, 1639. https://doi.org/10.3390/cryst13121639

Academic Editor: Benoit Heinrich

Received: 2 November 2023
Revised: 21 November 2023
Accepted: 22 November 2023
Published: 27 November 2023

1. Introduction

Nowadays, 2D flat panel displays are ubiquitous in our daily lives and serve as important tools for interacting with the world. They are extensively utilized in various commercial devices, including smartphones, tablets, laptops, smartwatches, micro-displays, and large-screen TV panels [1–3]. Despite the advanced stage of development in 2D display technology, achieving natural and vivid 3D displays remains the ultimate goal [4–6]. More recently, virtual reality (VR) and augmented reality (AR) have emerged as the most promising candidates for the next generation of mobile platforms, facilitating the advancement of 3D display technology [7–9]. Notably, Apple's introduction of the groundbreaking Apple Vision Pro headset in June 2023 has ignited researchers' enthusiasm towards AR/VR displays and 3D display technologies.

However, most of the current commercial devices, such as Apple Vision Pro, Microsoft HoloLens, Lumus, ODG smart glass, Meta, DigiLens, and Oculus Rift, employ conventional stereoscopy techniques to provide a 3D image [10,11]. In conventional 3D displays, two offset images are used to generate the depth information. The well-known issue lies in the conflict between vergence and accommodation [12,13], as depicted in Figure 1. In the real world, both the accommodation and vergence cues are accurately provided, as shown in Figure 1a. However, when viewing conventional stereoscopic 3D displays, our eyes are compelled to focus on the 2D screen in order to perceive the information clearly, while the 3D image appears at a distinct distance from the screen, as shown in Figure 1b. This mismatch between accommodation and vergence distances gives rise to visual fatigue, nausea, and other forms of discomfort. This is particularly evident in near-eye displays when users are fully immersed in a virtual environment using VR devices or observing 3D scenes in VR/AR devices after prolonged use. Thus, it is crucial to employ true 3D display technologies to display a natural 3D image [14].

To effectively address the problem of vergence–accommodation conflict (VAC), various true 3D display technologies have been proposed, including integral imaging displays [15], holography displays [16], super multi-view displays [17], Maxwellian viewing displays [18],

and multi-plane displays [19]. Over the past few decades, numerous liquid crystal (LC) devices have been proposed for these true 3D displays. Among them, liquid crystal display (LCD) and liquid crystal on silicon (LCoS) are widely utilized as light engines in various 3D displays. Moreover, various planar LC devices have been proposed as key optical components in both tabletop 3D displays and near-eye 3D displays, due to their excellent optical performance, electronic controllability, and extensive design flexibility.

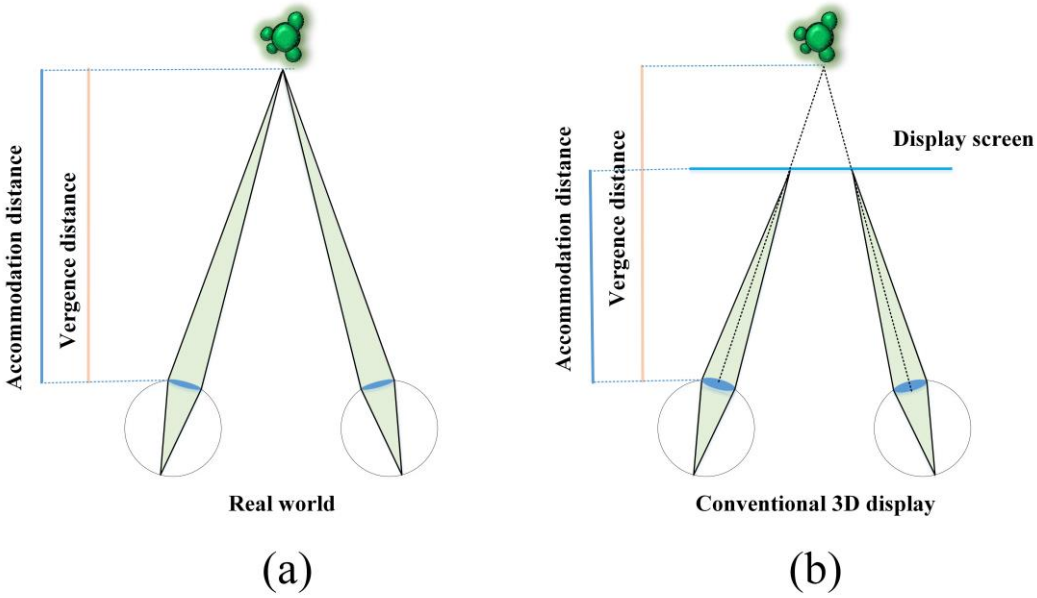

Figure 1. Vergence and accommodation conflict (VAC) problem. (**a**) Natural 3D visual experience in real world. (**b**) VAC in conventional displays.

In this review, we mainly focus on planar LC devices for true 3D display applications, discussing their working principles and properties. Firstly, we review recent advancements in multi-plane displays/varifocal displays based on LC devices, including LC scattering shutter, refractive LC lens, Pancharatnam–Berry (PB) phase LC lens, Alvarez tunable LC lens, cholesteric LC (CLC) film, and LC polarization switch. Next, we review the super multi-view display utilizing PB phase LC optical elements. Subsequently, we delve into a video-rate holographic display based on dye/quantum dot-doped LC devices. Additionally, we discuss integral imaging display based on LC lens arrays. Finally, we provide discussion and insights into future developments of LC devices for 3D displays.

2. Multi-Plane Displays Based on LC Devices

The multi-plane displays generate multiple 2D images positioned at different planes within the volume. This method provides the acceptable accommodation cues and solves the VAC problem in conventional 3D displays [19–21]. The straightforward way to achieve a multi-plane display involves utilizing a stack of transparent displays in space [22]. Many tunable optical components, such as liquid lens [23], deformable mirror [24,25], and LC devices have been proposed for utilization in multi-plane AR displays employing the time-multiplexing method [26–29]. Relevant research indicates that multi-plane display technology has the ability to achieve a continuous 3D scene with only six planes for AR applications [24], and this approach effectively strikes a balance between computational complexity and image quality, making it suitable for use in next-generation AR/VR devices. In the following sections, we review the applications of LC devices in different multi-plane systems.

2.1. Based on LC Scattering Shutter

In 2016, we proposed an optical see-through multi-plane AR display based on a stack of polymer-stabilized LC (PSLC) scattering shutters [19]. The normal mode PSLC scattering shutter is in a scattering state when the voltage is off, due to the refractive index mismatch in different domains, as shown in Figure 2b. When an external voltage is applied, the LC molecules are uniformly reoriented along the electric field, and the PSLC scattering shutter switches to a transparent state, as shown in Figure 2a. The formation of the polymer network significantly accelerates the response time of the PSLC to approximately 0.65 ms, enabling rapid switching of PSLC films in the system. Figure 2c shows the system configuration of the AR display based on PSLC film. The AR system comprises a quasi-collimated projector, a stack of PSLC films, an ocular lens, and an optical combiner. The PSLC films maintain transparency except for one film in the scattering state at any given moment, while simultaneously projecting a corresponding 2D slice onto it. To ensure clear display of the projection image at different planes, a quasi-collimated projector should be employed. Figure 2d is a quasi-collimated projector consisting of three lenses (l_1, l_2, and l_3), a pinhole, and a commercial projector. The lens l_1 forms a real image of the original image at the front focal plane of l_2. A pinhole is positioned at the back focal plane of l_2 where the beam diameter is minimized. As this pinhole location also serves as the front focal plane of lens l_3, the output image light becomes quasi-collimated with a single angular spectrum, thereby providing a large depth of field. Consequently, 2D images on each PSLC shutter consistently exhibit sharpness and uniformity in size. Then, the virtual image can be perceived by the viewer after the magnification of the ocular lens. A four-plane 60 Hz AR display prototype utilizing a 360 Hz digital mirror device (DMD) was implemented in our experiment. Figure 2e–h showcase the images captured at four different depths, indicating that the system provides accurate depth cues.

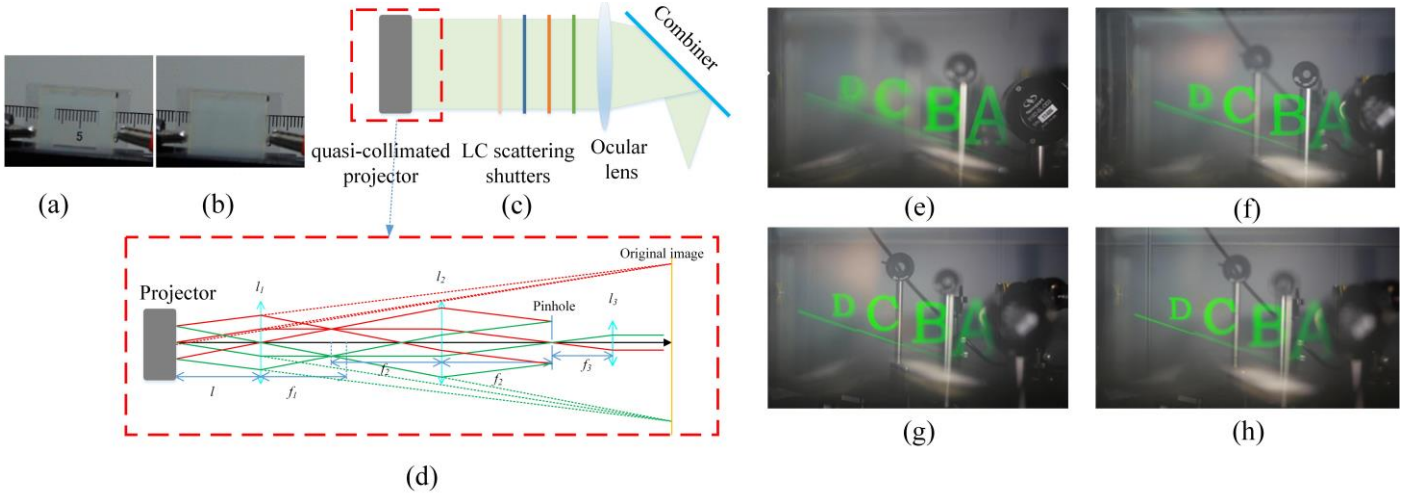

Figure 2. (**a**,**b**) PSLC film in a transparent state and a scattering state when the applied voltage is on and off [19], respectively. (**c**) Optical scheme of the AR system based on PSLC scattering shutters. (**d**) Ray tracing diagram of the quasi-collimated projector. (**e**–**h**) Demonstration of the AR display prototype with four letters "A,B,C,D" when focusing the camera at 30 cm, 50 cm, 80 cm, and 500 cm [19], respectively. (**a**,**b**,**e**–**h**) adapted with permission from Ref. [19], Wiley.

In this multi-plane AR display system based on PSLC scattering shutters, only one film is in a scattering state at one moment. To reduce power consumption, we proposed a multi-plane AR display system based on reverse mode PSLC scattering shutters using a negative LC material ($\Delta\varepsilon < 0$) in 2018. Because only one reverse mode PSLC film needs an applied voltage at one moment, the power consumption of the reverse mode PSLC-based system is reduced to $1/(N-1)$ compared to that of a normal mode PSLC-based system [28].

2.2. Based on Refractive LC Lens

The multi-plane display can be achieved by adjusting the focal length of the tunable lens, also known as a varifocal display [30–33]. By rapidly varying optical power of the tunable lens, a continuous 3D scene can be reconstructed. In 2015, Chen et al. proposed an AR system using a refractive LC lens [32]. They adopted a double-layered refractive LC lens structure, as shown in Figure 3b. When $V_1 = V_2$, the optical power of the refractive LC lens is zero because the LC molecules are uniformly aligned. When $V_1 < V_2$, the optical power of the refractive LC lens is negative, because the LC molecules near the center are more perpendicular, while those near the edge are more parallel. Conversely, when $V_1 > V_2$, the optical power of the refractive LC lens is positive. The optical power of the refractive LC can continuously change from −1.34 to +1.82 D with applied voltages. The rise and fall response times of the refractive LC lens are 1.7 and 3.1 s. The prototype comprises a refractive LC lens, a concave mirror, an optical combiner, and a spatial light modulator (SLM), as illustrated in Figure 3a. By manipulating the applied voltages (V_1 and V_2) on the refractive LC lens, the virtual image planes can be tuned from 42 to 360 cm, while the real image can be tuned from 27 to 52 cm on the other side. Due to its relatively slow response time, the system is incapable of operating at video rate.

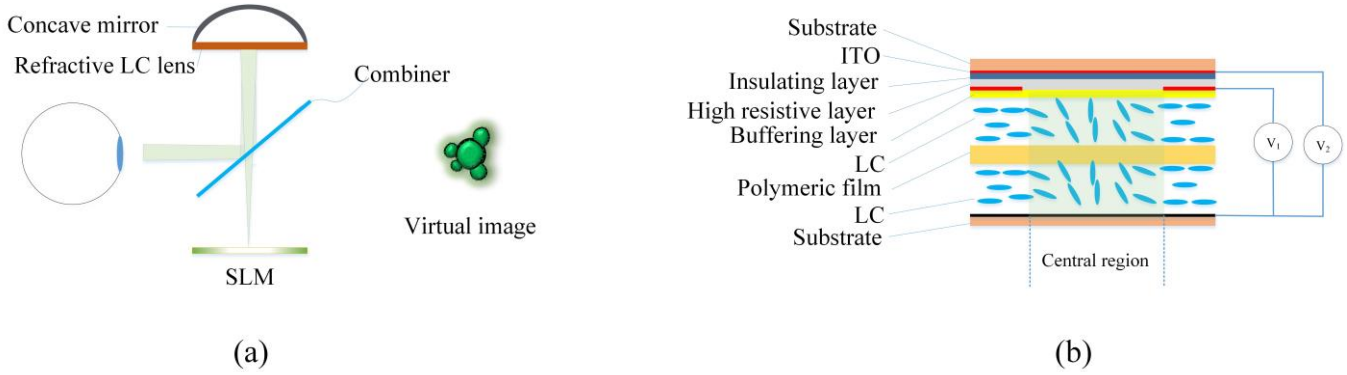

Figure 3. (**a**) Multi-plane display based on a refractive LC lens. (**b**) Structure of the refractive LC lens.

2.3. Based on Pancharatnam–Berry Phase LC Lens

Over the past few decades, Pancharatnam–Berry LC (PBLC) devices have undergone significant development in various fields due to their exceptional ability to manipulate the phase and polarization of light [34,35]. By precisely controlling the alignment of LC molecules with photoalignment azo dye materials [36,37]. PBLC devices can achieve accurate modulation of incident light's phase and polarization. This capability has found extensive use in diverse fields such as lens, grating, holography, and vortex beams [38]. Additionally, PBLC offers advantages such as compactness, high efficiency, and polarization selectivity [39–41].

The PBLC lens exhibits polarization sensitivity and demonstrates opposite optical power for right-handed circularly polarized (RCP) and left-handed circularly polarized (LCP) light. Thus, the optical power of a PBLC lens can be switched between two states. There are mainly two ways to drive the PBLC lens: (1) directly applying a voltage across the LC cell, and (2) adding an external polarization switch to select the input polarization between LCP and RCP. Here, we focus on the multi-plane display based on the active driving method. In 2017, Lee et al. built a dual-plane AR system using the PBLC lens [33]. In 2019, we proposed a multi-plane AR system based on two fast-response PBLC lenses [40], as depicted in Figure 4. To fabricate the fast response PBLC lens, we first utilized a non-interferometric single-exposure photoalignment technique to fabricate an alignment layer. Then, polymer networks were formed in the LC cell through UV curing. The PBLC lens exhibited a response time of ~0.8 ms and achieved a high diffraction efficiency of ~90%. By stacking two PBLC lenses, four discrete optical powers (f = 50 cm, 100 cm, −100 cm, and ∞) can be realized with two applied voltages. We demonstrated a four-plane AR

prototype, rendering "SJTU" at distances of 28 cm, 40 cm, 67 cm, and 200 cm, as captured in Figure 4i–l.

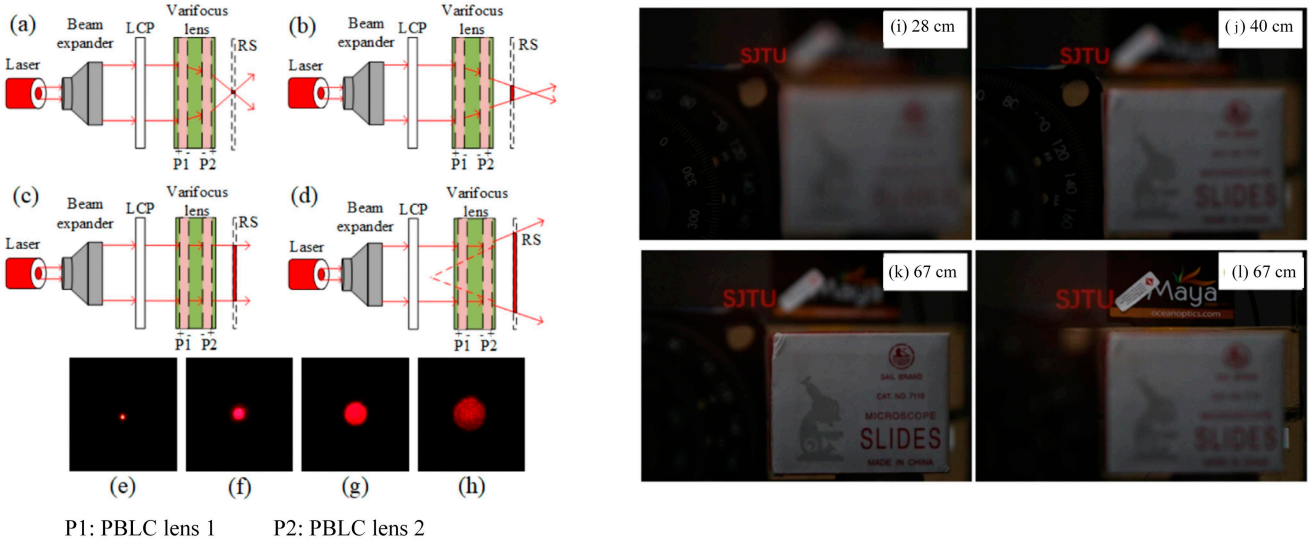

Figure 4. Four-plane display based on two PBLC lenses. (**a**–**d**) Four modes: f = 50 cm, 100 cm, ∞, and −100 cm when the applied voltages on P1 and P2 are off | off, off | on, on | on, and on | off, respectively [40]. (**e**–**h**) Beam spots on the RS when f = 50 cm, 100 cm, ∞, and −100 cm, respectively. RS: receiving screen [40]. (**i**–**l**) Four letters, "SJTU", are rendered at distances of 28 cm, 40 cm, 67 cm, and 200 cm [40]. (**a**–**l**) adapted with permission from Ref. [40], Optica Publishing Group.

2.4. Based on Planar Alvarez Tunable LC Lens

The exceptional design flexibility of PBLC design enables the achievement of any desired phase distribution through the single-exposure photoalignment technique employing an SLM. The Alvarez lens is a tunable lens consisting of two sub-elements, allowing for continuous focal length adjustment through lateral displacement [41]. Therefore, the Alvarez tunable lens can serve as the key optical component in multi-plane display system [31]. However, the conventional freeform Alvarez lens is difficult to manufacture and usually has a bulky size for compact AR devices. In 2022, Chen et al. from our group proposed a planar PB Alvarez LC lens for multi-plane AR applications, significantly reducing the manufacturing complexity of the Alvarez lens [42]. The Alvarez LC lens offers an optical power ranging from −1.4 D to 1.4 D at 532 nm when a lateral shift ranging from −5 mm to 5 mm. By laterally shifting the sub-elements of the Alvarez lens, as illustrated in Figure 5b, virtual images at different distances can be achieved. Figure 5a shows an AR letter "G" displayed at different depths by the prototype. The virtual image becomes sharp when the camera adjusts its focus to the correct depth. Consequently, the system is capable of providing accurate depth cues. However, the proposed method presents challenges in achieving a dynamic 3D display due to the mechanical movement required for two sub-elements.

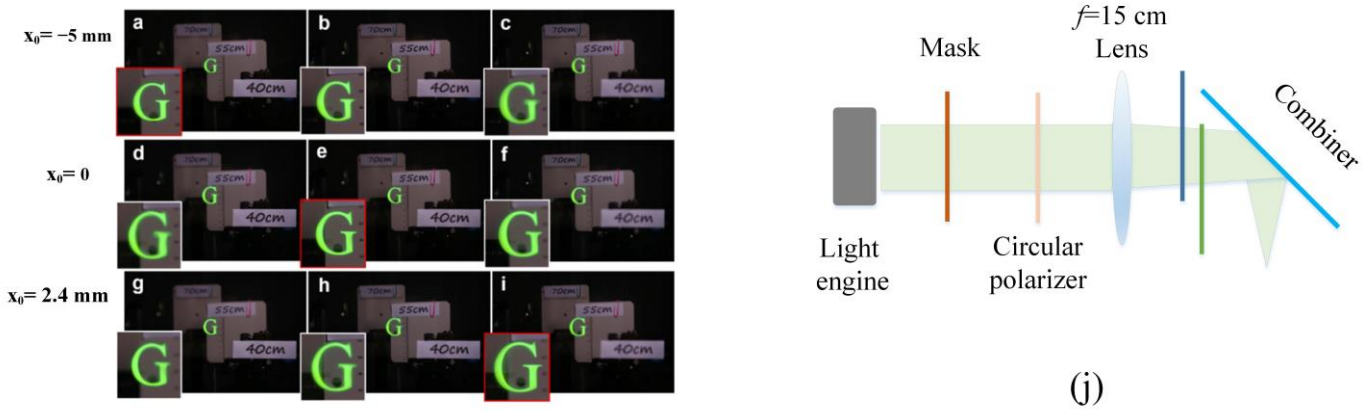

Figure 5. (**a**–**c**) Virtual image "G" is rendered at 40 cm with a lateral shift of x_0 = −5 mm when focusing the camera at 40 cm, 55 cm, and 70 cm [42], respectively. (**d**–**f**) Virtual image "G" is rendered at 55 cm with a lateral shift of x_0 = 0 when focusing the camera at 40 cm, 55 cm, and 70 cm [42], respectively. (**g**–**i**) Virtual image "G" is rendered at 70 cm with a lateral shift of x_0 = 2.4 mm when focusing the camera at 40 cm, 55 cm, and 70 cm [42], respectively. (**j**) Scheme of multi-plane display based on planar Alvarez tunable LC lens. (**a**–**i**) adapted with permission from Ref. [42], Optica Publishing Group.

2.5. Based on CLC Films

The CLC film exhibits strong polarization selectivity, reflecting one circularly polarized light completely and transmitting the other nearly 100% [43–45]. In our experiment, we fabricated two reflective CLC cells with opposite handedness in order to distinguish between the RCP and LCP light by manipulating the optical distances [26]. A polarization switch combined with a linear polarizer, a TN LC cell, and a λ/4 plate was employed to generate the RCP and LCP light sources, as shown in Figure 6a. Thus, the RCP and LCP can be formed at two different depths which realize the multi-plane function. As shown in Figure 6b–e, the color image "flower" was rendered at distances of 20 cm and 130 cm from the camera. To achieve a continuous 3D image, we devised a multi-plane AR display by alternately stacking switchable λ/2 plates and CLC films. However, achieving full-color display with a CLC cell remains challenging in this system, even with the use of large birefringence (Δn~0.4) LC material.

2.6. Based on LC Polarization Switch

The LC polarization switch is a commonly used device in multi-plane displays [46]. The primary LC device employed is a twisted nematic (TN) LC cell [47,48], which alters the polarization of linearly polarized light. As previously discussed, an external polarization switch can be added to select the input polarization between LCP and RCP, thereby switching the PBLC lens between focusing and defocusing states. Additionally, CLC films also require an LC polarization switch. Furthermore, when combined with other polarization-dependent devices, such as a polarizing beam splitter (PBS) [27] and Savart plate [49], the LC polarization switch enables the realization of multi-plane functionality. In 2016, Lee et al. presented a proof-of-concept dual-focal near-eye display system utilizing polarization-dependent PBS to separate the optical paths of two linearly polarized lights [27], as shown in Figure 7. Subsequently, by incorporating λ/4 plates and employing two mirrors in conjunction with the PBS, distinct optical distances are created, resulting in the formation of two depth images.

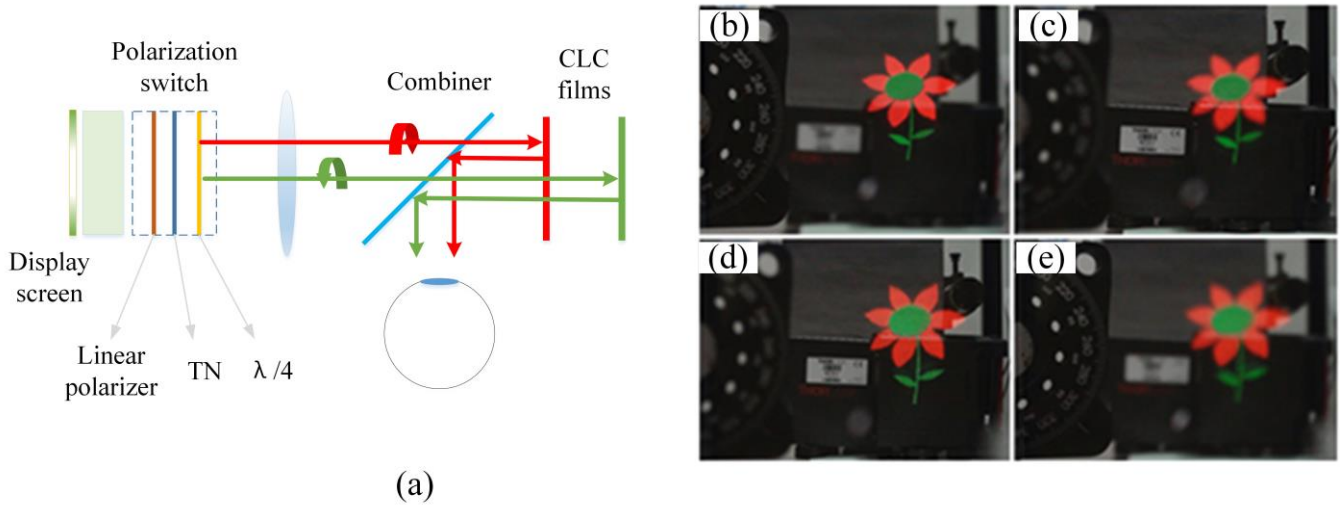

Figure 6. (**a**) AR display based on two CLC films with opposite handedness. Red arrow is the LCP light, and green arrow is RCP light. (**b**,**c**) Color image is rendered at 20 cm when focusing the camera at 20 cm and 130 cm, respectively [26]. (**d**,**e**) Color image is rendered at 130 cm when focusing the camera at 130 cm and 20 cm [26], respectively. (**b**–**e**) adapted with permission from Ref. [26], Optica Publishing Group.

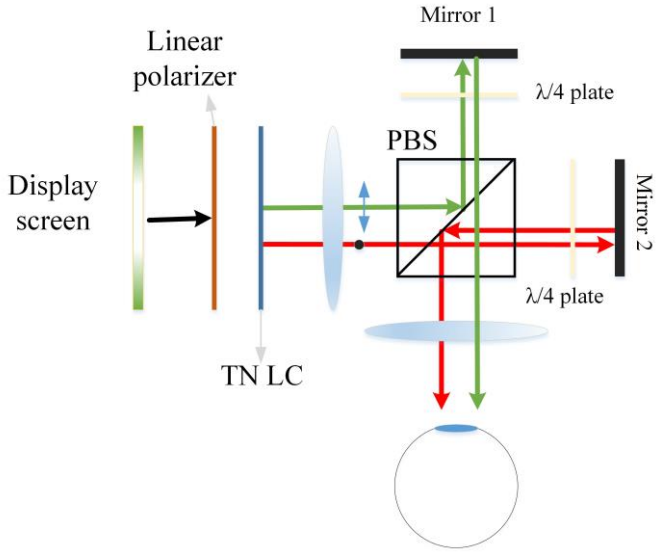

Figure 7. Dual-plane AR display system utilizing a LC polarization switch and PBS.

3. Super Multi-View Displays

A super multi-view (SMV) display is a true 3D display technology that effectively stimulates the eye to focus on a virtual 3D image [5,50,51]. To generate more natural visual effects in 3D displays, SMV displays use an extremely large number of views (for example, 256 views) to create a natural 3D experience for tabletop 3D displays [17,52]. In this technique, the interval between viewing zones is much smaller than the pupil diameter (at least two views enter the pupil simultaneously), allowing for multiple rays passing through the same point in space to pass through the eye pupil simultaneously. Consequently, our eyes can effortlessly focus on that specific point. For near-eye displays, the requirement for the number of views is significantly reduced, as it only needs sufficient coverage around the pupil [53,54].

Recently, in 2022, Wang et al. from our group proposed an SMV AR display system based on PBLC devices [55], as shown in Figure 8a. Figure 8b,c shows two kinds of PBLC grating array. Gratings of different regions in the PBLC grating have different vector

orientations or grating periods. Thus, it can generate light beams in different directions (3 × 1 and 3 × 2 directions). In our experiment, the diffraction efficiencies of the PBLC gratings were nearly 90%, significantly enhancing the image quality. The interval between the light beams at the pupil position is approximately 2 mm, allowing for light rays from different views to enter the human eye simultaneously. Finally, an SMV display prototype was successfully implemented.

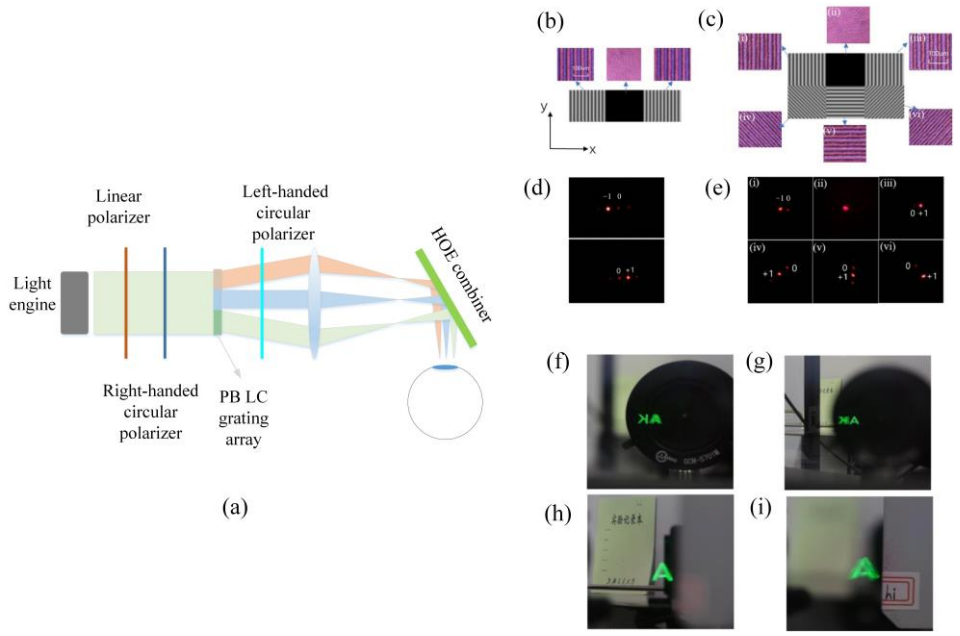

Figure 8. (**a**) SMV display based on PBLC grating array. (**b**,**c**) Microscopic images of 1D/2D PBLC grating arrays [55]. (**d**,**e**) Diffraction patterns from different regions of the 1D/2D PB LC grating arrays [55]. (**f**,**g**) SMV display with 1D PBLC grating when camera focusing at 20 cm and 160 cm. (**h**,**i**) SMV display with 2D PBLC when focusing camera at different distances [55]. (**b**–**i**) adapted with permission from Ref. [55], Creative Commons.

The proof-of-concept prototype of SMV display was implemented based on the 1D PBLC grating array. As shown in Figure 8f,g, the virtual letter "A" is rendered at a distant location, while the virtual letter "K" is rendered close to the eye. Figure 8h,i illustrate the generation of letter "A" at a far distance when employing the 2D PBLC grating array. The system provides full monocular focus cues without VAC problem, ensuring a natural 3D experience for the viewer. However, considering the movement of eyeballs, the current number of views is still insufficient. To enhance the visual experience, it is necessary to further increase the number of views. Moreover, the achievement of color display may encounter challenges due to the wavelength-dependent characteristics of PBLC devices.

4. Holographic Displays

Holographic displays are considered the ultimate display technology due to their ability to provide all the depth cues of an object, enabling a 3D experience without visual fatigue [56,57]. Currently, holographic displays based on LC technology predominantly employ SLMs as light engines and construct 3D images through computer-generated holograms [58,59]. However, these displays face challenges such as limited diffraction angle, poor scalability, unwanted diffractive orders, and zero-order light due to the relatively large pixel size, small display size, and low resolution of existing SLM devices.

In 2013, Li et al. from our group proposed a video-rate holographic display using an azo dye-doped LC device [60]. The DR1 is an azo dye material capable of undergoing a reversible photochemical transition between the *trans* and *cis* states. Under laser irradiation, DR1 molecules change from their original oblong-shaped *trans* state to a bent-shaped

cis state, as shown in Figure 9a. The unstable *cis* state of azo molecules can transform back to the *trans* state in darkness. The alteration in the orientation of azo molecules also induces a change in the alignment of LC molecules, leading to variations in refractive index and the formation of a refractive index grating, as shown in Figure 9a. In the system, the interference of two recording beams generates a holographic pattern, leading to the refractive index grating. A real-time 25 Hz holographic display was demonstrated based on a dye-doped LC device. In 2016, our group proposed a dynamic holographic display based on a quantum dot (ZnS/InP)-doped LC device [61,62]. Under the influence of laser irradiation, quantum dots efficiently absorb photons and generate free charge. Figure 9b depicts that when a voltage is applied, the photo-excited charge creates a local space field. Consequently, a refractive index grating is induced by the nonuniform distribution of interference intensity. The optical setup is shown in Figure 9c. The dynamic binary images, generated using a computer, are loaded onto an amplitude SLM at a refresh rate of 25 Hz. The object beam with image information is illuminated onto the LC cell. A 460 nm laser is used to provide coherent reference and object beams, with s-polarization set for both. The intensity ratio of the object beam and reference beam is approximately 1:1. Under the illumination of two reference and object beams, electrons and holes separate and transport along the grating wave vector when a DC voltage is applied. This creates a nonuniform space charge field that induces spatially modulated reorientation of LC molecules and periodic refractive index modulation. When the two reference and object beams are removed, the distribution of photoinduced charges becomes uniform, thereby eliminating the grating. In the experiment, both the build-up time and decay time of the grating are ~4 ms. Therefore, we can implement a video-rate holographic display. Based on the quantum dot-doped LC device, Figure 9d shows a sequence of snapshots of the real-time video-rate 25 Hz holographic display system using three R,G,B reading beams.

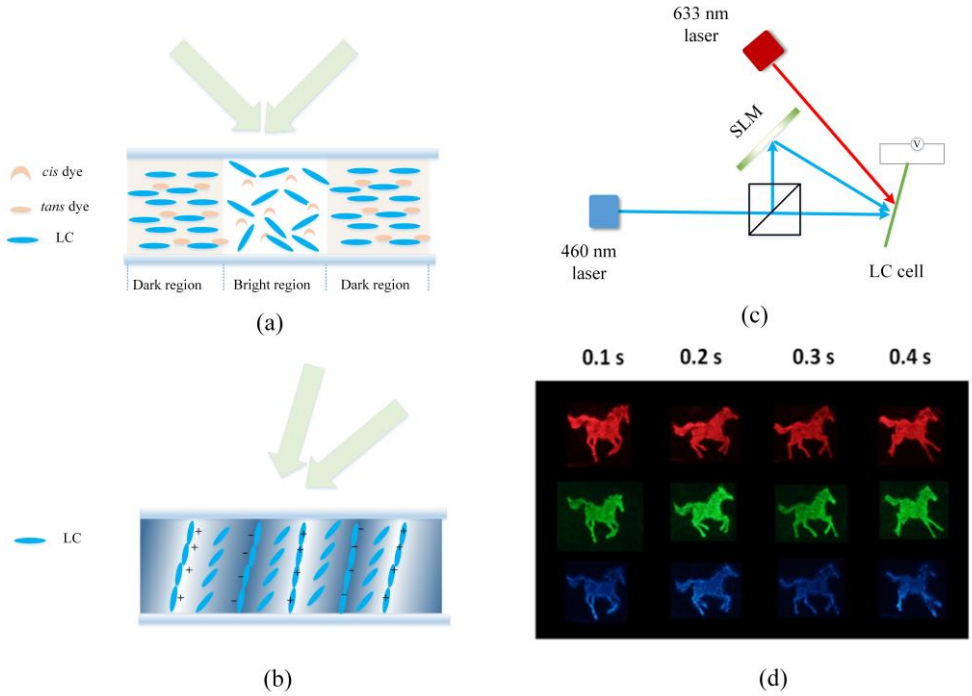

Figure 9. (**a**) Principle of the azo dye-doped LC device. (**b**) Principle of the quantum dot-doped LC device. (**c**) Schematic of the real-time holographic display system based on LC device. (**d**) Snapshots using three R,G,B reading beams [62]. (**d**) adapted with permission from Ref. [62], Optica Publishing Group.

5. Integral Imaging Based on LC Lens Array

The integral imaging 3D display technique effectively addresses the VAC issue by providing continuous depth information. The main structure of the integral imaging scheme

comprises a high-resolution 2D display screen and a lens array, as shown in Figure 10a. Each lens is associated with a 2D elemental picture providing a distinct perspective of the 3D scene. The LC devices could serve as either the high-resolution display screen or the lens array components. As LCDs are commonly used in 3D systems, we mainly focus on the integral imaging display based on LC lens arrays.

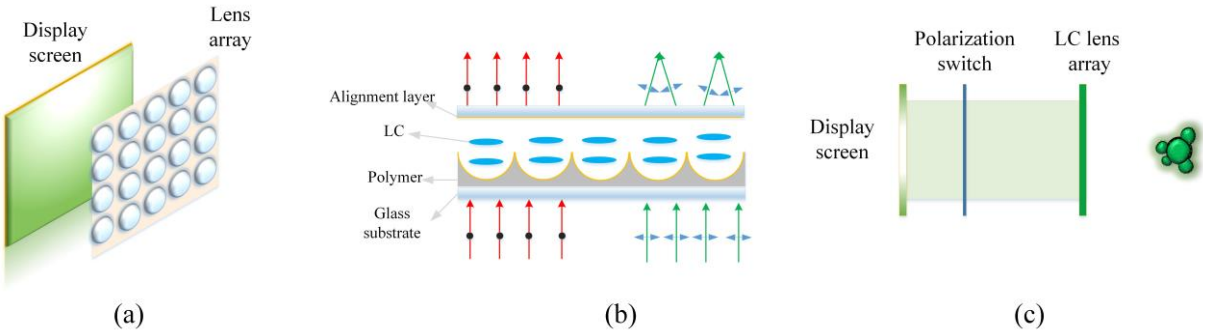

Figure 10. (**a**) Schematic of the integral imaging. (**b**) Polarization-dependent LC lens array. (**c**) Schematic of the integral imaging based on LC lens array.

The fundamental operational mechanism of the LC lens array involves spatial variation of the refractive index across the LC layer. This can be realized by patterned electrodes [63–65], patterned polymer networks [66], PBLC devices [67], and other materials [68,69]. Various methods have been proposed for integral imaging display based on LC lens array [70–72]. For example, in 2021, Li et al. proposed a compact 2D/3D integral imaging display based on an LC lens array [70]. The basic structure of the LC lens array is composed of two substrates, LC, a planoconcave polymer layer, and an alignment layer, as shown in the Figure 10b. The ordinary refractive index of the LC material closely matches that of the polymer layer, allowing for the LC lens to directly transmit y-polarized light while focusing on x-polarized light. Therefore, this LC lens exhibits a polarization-dependent property. By changing the direction of input polarized light, the system is capable of switching between 2D and 3D display modes, as shown in Figure 10c. The LC lens array has a size of 45 mm × 40 mm. Each sub-lens has a focal length of 1.3 mm and a diameter of 1 mm. In this 3D display mode, the resolution is reduced to 45 × 40 pixels. Although integral imaging display can provide full depth cues, the resolution of the system is relatively low, greatly reducing the quality of 3D images.

A commonly employed method for implementing LC lens arrays involves the utilization of patterned electrodes. In 1991, Patel et al. presented an electrically controlled Fresnel lens array (8 × 8) that used patterned electrodes [63]. The LC lens array has a low driving voltage of ~2V and a diffractive efficiency of 34%. In 2014, Chang et al. proposed a 3D display based on LC lens array using stripe electrodes [64]. In the 3D mode, a gradient electric field distribution can be formed when an external voltage is applied, allowing for the generation of a spatial variation in refractive index across the LC layer. They successfully implemented a 3D image with horizontal and vertical views. Recently, Zhang et al. proposed an integral imaging display based on an electrically high-resistance LC lens array in 2020 [72]. Figure 11a illustrates the utilization of circular hole aluminum (Al) electrodes to generate a gradient electric field, enabling the achievement of spatial variation in refractive index across the LC layer. The LC lens array consists of an Al patterned electrode, a high-resistance layer, LC layer, two alignment layers, ITO layer, and two glass substrates, as shown in Figure 11b. They implemented a 3D display with different depths using a smartphone panel (320 × 180 elemental pictures) and the LC lens arrays. The driving voltage of the LC lens array is about 2.8 V.

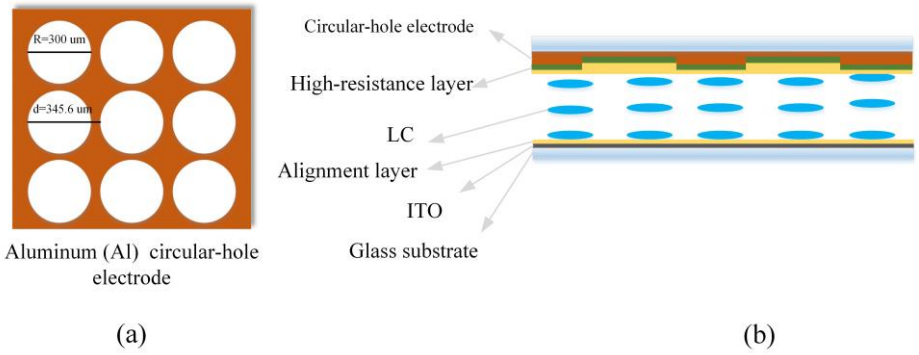

Figure 11. (**a**) Al circular hole electrode. (**b**) Structure of LC lens array using patterned electrode.

The LC lens array boasts features such as a lightweight design, compact size, low power consumption, and a tunable optical power. And it enables switchable 2D/3D display functionality. However, the integral imaging display has a limited depth range and requires a tradeoff between the depth of field and spatial resolution.

6. Conclusions and Prospects

In this review, we briefly reviewed the recent advancements in the applications of LC devices for true 3D displays. Initially, we introduced multi-plane display technologies based on LC devices. Tunable LC devices such as LC scattering shutter, refractive LC lens, PBLC lens, Alvarez tunable LC lens, CLC film, and LC polarization switch for 3D displays were reviewed. Additionally, we discussed the super multi-view technology based on PBLC grating arrays and holographic display utilizing doped LC materials. Furthermore, integral imaging displays based on LC lens arrays were also reviewed. The pros and cons of these true 3D displays based on LC devices are summarized in Table 1. The aforementioned approaches are all dedicated to solving the VAC problem and enabling a natural 3D experience without visual fatigue. The utilization of planar LC optics offers excellent optical performance characterized by an ultrathin form factor, high efficiency, fast response time, polarization-dependent behaviors, wavelength-dependent behaviors, and a high degree of design freedom. These outstanding characteristics enable the application of LC devices in various 3D systems.

Table 1. Pros and cons of some true 3D display-based LC devices.

True 3D Displays	LC Devices	Pros	Cons
Multi-plane display	LC scattering shutter [19,28]	Fast response time	High driving voltage
	Refractive LC lens [32]	Continuous optical power change	Slow response time, small aperture
	PB phase LC lens [33,40]	Fast response time, polarization dependence, compact	Chromatic dispersion
	Planar Alvarez tunable lens [42]	Planar device, large adjustment range, compact	Require lateral displacement
	CLC films [26]	Polarization dependence	Require large Δn LC material to cover the visible light
	LC polarization switch [27,49]	Fast response time	Require other polarization devices
Super multi-view display	PB grating array [55]	High diffraction efficiency, views is significantly reduced	Chromatic dispersion
Holographic display	Azo dye-doped LC [60]	Video rate	Two-beam interference
	Quantum dot doped LC [61,62]	Video rate, highly photorefractive	Two-beam interference
	SLM	/	/
Integral imaging display	LC lens array [70,72]	Lightweight design, tunable optical power	Limited depth range, low resolution
	LCD	/	/

However, certain limitations of LC devices need to be addressed. For example, the PSLC film exhibits a high driving voltage, refractive LC lens has a slow response time, PB LC devices suffer from chromatic dispersion, and some LC devices have small apertures. Additionally, in order to achieve a vivid holographic display and integral imaging display, the resolution requirements for LC-based SLM or LCD screens far exceed current capabilities. As technology continues to evolve, there is an increasing emphasis on overcoming current limitations and enhancing the overall performance of these LC devices. The tunable metasurface based on LC material has the potential to reduce the pixel size of SLMs and increase display resolutions [73]. The realization of achromatic LC optics may be achieved through innovative design utilization [74] and advanced LC formulations. Furthermore, ongoing innovations in manufacturing processes are expected to result in more ultrathin compact LC devices, thereby making these solutions more accessible for AR/VR wearable devices. Although there are still many challenges to overcome in practical devices, true 3D displays utilizing LC devices hold significant promise for advancing both tabletop and near-eye 3D devices in the future. We believe that LC devices possess great potential for future 3D display applications, particularly in AR and VR applications, facilitating the development of compact and lightweight headsets.

Author Contributions: Writing—review and editing, S.L., Y.L. and Y.S. All authors have read and agreed to the published version of the manuscript.

Funding: This research was funded by the National Natural Science Foundation of China, 62105203 and 62075127.

Data Availability Statement: Not applicable.

Conflicts of Interest: The authors declare no conflict of interest.

References

1. Schadt, M. Liquid crystal materials and liquid crystal displays. *Annu. Rev. Mater. Sci.* **1997**, *27*, 305–379. [CrossRef]
2. Geffroy, B.; Le Roy, P.; Prat, C. Organic light-emitting diode (OLED) technology: Materials, devices and display technologies. *Polym. Int.* **2006**, *55*, 572–582. [CrossRef]
3. Yang, D.-K.; Wu, S.-T. *Fundamentals of Liquid Crystal Devices*; John Wiley & Sons: Hoboken, NJ, USA, 2014.
4. Dodgson, N.A. Autostereoscopic 3D displays. *Compute* **2005**, *38*, 31–36. [CrossRef]
5. Geng, J. Three-dimensional display technologies. *Adv. Opt. Photonics* **2013**, *5*, 456–535. [CrossRef] [PubMed]
6. Yang, L.; Dong, H.; Alelaiwi, A.; Saddik, A.E. See in 3D: State of the art of 3D display technologies. *Multimed. Tools Appl.* **2016**, *75*, 17121–17155. [CrossRef]
7. Hsiang, E.-L.; Yang, Z.; Yang, Q.; Lai, P.-C.; Lin, C.-L.; Wu, S.-T. AR/VR light engines: Perspectives and challenges. *Adv. Opt. Photonics* **2022**, *14*, 783–861. [CrossRef]
8. Xiong, J.; Hsiang, E.-L.; He, Z.; Zhan, T.; Wu, S.-T. Augmented reality and virtual reality displays: Emerging technologies and future perspectives. *Light Sci. Appl.* **2021**, *10*, 216. [CrossRef]
9. Zhan, T.; Yin, K.; Xiong, J.; He, Z.; Wu, S.-T. Augmented reality and virtual reality displays: Perspectives and challenges. *Iscience* **2020**, *23*, 101397. [CrossRef]
10. Hua, H.; Javidi, B. A 3D integral imaging optical see-through head-mounted display. *Opt. Express* **2014**, *22*, 13484–13491. [CrossRef]
11. Park, J.-H.; Lee, B. Holographic techniques for augmented reality and virtual reality near-eye displays. *Light Adv. Manuf.* **2022**, *3*, 137–150. [CrossRef]
12. Hoffman, D.M.; Girshick, A.R.; Akeley, K.; Banks, M.S. Vergence–accommodation conflicts hinder visual performance and cause visual fatigue. *J. Vision* **2008**, *8*, 33. [CrossRef] [PubMed]
13. Shibata, T.; Kim, J.; Hoffman, D.M.; Banks, M.S. Visual discomfort with stereo displays: Effects of viewing distance and direction of vergence-accommodation conflict. In *Stereoscopic Displays and Applications XXII*; SPIE: San Francisco, CA, USA, 2011.
14. Ren, H.; Ni, L.X.; Li, H.F.; Sang, X.Z.; Gao, X.; Wang, Q.H. Review on tabletop true 3D display. *J. Soc. Inf. Disp.* **2020**, *28*, 75–91. [CrossRef]
15. Zhang, W.; Sang, X.; Gao, X.; Yu, X.; Gao, C.; Yan, B.; Yu, C. A flipping-free 3D integral imaging display using a twice-imaging lens array. *Opt. Express* **2019**, *27*, 32810–32822. [CrossRef] [PubMed]
16. Zhao, R.; Sain, B.; Wei, Q.; Tang, C.; Li, X.; Weiss, T.; Huang, L.; Wang, Y.; Zentgraf, T. Multichannel vectorial holographic display and encryption. *Light Sci. Appl.* **2018**, *7*, 95. [CrossRef] [PubMed]
17. Takaki, Y.; Nago, N. Multi-projection of lenticular displays to construct a 256-view super multi-view display. *Opt. Express* **2010**, *18*, 8824–8835. [CrossRef]

18. Zhang, Q.; Song, W.; Liu, Y.; Wang, Y. Design and implementation of an optical see-through near-eye display combining Maxwellian-view and light-field methods. *Opt. Commun.* **2022**, *510*, 127833. [CrossRef]
19. Liu, S.; Li, Y.; Su, Y. Multiplane displays based on liquid crystals for AR applications. *J. Soc. Inf. Disp.* **2020**, *28*, 224–240. [CrossRef]
20. Tan, G.; Zhan, T.; Lee, Y.-H.; Xiong, J.; Wu, S.-T. Polarization-multiplexed multiplane display. *Opt. Lett.* **2018**, *43*, 5651–5654. [CrossRef]
21. Hu, X.; Hua, H. Design and assessment of a depth-fused multi-focal-plane display prototype. *J. Soc. Inf. Disp.* **2014**, *10*, 308–316. [CrossRef]
22. Rolland, J.P.; Krueger, M.W.; Goon, A. Multifocal planes head-mounted displays. *Appl. Opt.* **2000**, *39*, 3209–3215. [CrossRef]
23. Liu, S.; Hua, H. Time-multiplexed dual-focal plane head-mounted display with a liquid lens. *Opt. Lett.* **2009**, *34*, 1642–1644. [CrossRef] [PubMed]
24. Hu, X.; Hua, H. High-resolution optical see-through multi-focal-plane head-mounted display using freeform optics. *Opt. Express* **2014**, *22*, 13896–13903. [CrossRef] [PubMed]
25. Dunn, D.; Chakravarthula, P.; Dong, Q.; Fuchs, H. Mitigating vergence-accommodation conflict for near-eye displays via deformable beamsplitters. In *Digital Optics for Immersive Displays*; SPIE: Strasbourg, France, 2018.
26. Chen, Q.; Peng, Z.; Li, Y.; Liu, S.; Zhou, P.; Gu, J.; Lu, J.; Yao, L.; Wang, M.; Su, Y. Multi-plane augmented reality display based on cholesteric liquid crystal reflective films. *Opt. Express* **2019**, *27*, 12039–12047. [CrossRef] [PubMed]
27. Lee, Y.-H.; Peng, F.; Wu, S.-T. Fast-response switchable lens for 3D and wearable displays. *Opt. Express* **2016**, *24*, 1668–1675. [CrossRef] [PubMed]
28. Liu, S.; Li, Y.; Zhou, P.; Chen, Q.; Su, Y. Reverse-mode PSLC multi-plane optical see-through display for AR applications. *Opt. Express* **2018**, *26*, 3394–3403. [CrossRef] [PubMed]
29. Zhan, T.; Lee, Y.-H.; Tan, G.; Xiong, J.; Yin, K.; Gou, F.; Zou, J.; Zhang, N.; Zhao, D.; Yang, J. Pancharatnam–Berry optical elements for head-up and near-eye displays. *JOSA B* **2019**, *36*, D52–D65. [CrossRef]
30. Suyama, S.; Date, M.; Takada, H. Three-dimensional display system with dual-frequency liquid-crystal varifocal lens. *Jpn. J. Appl. Phys.* **2000**, *39*, 480. [CrossRef]
31. Wilson, A.; Hua, H. Design and demonstration of a vari-focal optical see-through head-mounted display using freeform Alvarez lenses. *Opt. Express* **2019**, *27*, 15627–15637. [CrossRef]
32. Chen, H.-S.; Wang, Y.-J.; Chen, P.-J.; Lin, Y.-H. Electrically adjustable location of a projected image in augmented reality via a liquid-crystal lens. *Opt. Express* **2015**, *23*, 28154–28162. [CrossRef]
33. Lee, Y.-H.; Tan, G.; Zhan, T.; Weng, Y.; Liu, G.; Gou, F.; Peng, F.; Tabiryan, N.V.; Gauza, S.; Wu, S.-T. Recent progress in Pancharatnam–Berry phase optical elements and the applications for virtual/augmented realities. *Opt. Data Process. Storage* **2017**, *3*, 79–88. [CrossRef]
34. Zou, J.; Luo, Z.; Zhao, E.; Rao, Y.; Wu, S.-T. Ultracompact virtual reality system with a Pancharatnam–Berry phase deflector. *Opt. Express* **2022**, *30*, 39652–39662. [CrossRef] [PubMed]
35. Shteyner, E.A.; Srivastava, A.K.; Chigrinov, V.G.; Kwok, H.-S.; Afanasyev, A.D. Submicron-scale liquid crystal photo-alignment. *Soft Matter* **2013**, *9*, 5160–5165. [CrossRef]
36. Guo, Q.; Srivastava, A.K.; Chigrinov, V.G.; Kwok, H.S. Polymer and azo-dye composite: A photo-alignment layer for liquid crystals. *Liq. Cryst.* **2014**, *41*, 1465–1472. [CrossRef]
37. Lin, T.; Xie, J.; Zhou, Y.; Zhou, Y.; Yuan, Y.; Fan, F.; Wen, S. Recent advances in photoalignment liquid crystal polarization gratings and their applications. *Crystals* **2021**, *11*, 900. [CrossRef]
38. Xiong, J.; Wu, S.-T. Planar liquid crystal polarization optics for augmented reality and virtual reality: From fundamentals to applications. *eLight* **2021**, *1*, 3. [CrossRef]
39. Zou, J.; Zhan, T.; Xiong, J.; Wu, S.-T. Broadband wide-view Pancharatnam–Berry phase deflector. *Opt. Express* **2020**, *28*, 4921–4927. [CrossRef]
40. Li, S.; Liu, Y.; Li, Y.; Liu, S.; Chen, S.; Su, Y. Fast-response Pancharatnam-Berry phase optical elements based on polymer-stabilized liquid crystal. *Opt. Express* **2019**, *27*, 22522–22531. [CrossRef]
41. Han, Z.; Colburn, S.; Majumdar, A.; Böhringer, K.F. MEMS-actuated metasurface Alvarez lens. *Microsyst. Nanoeng.* **2020**, *6*, 79. [CrossRef]
42. Chen, S.; Lin, J.; He, Z.; Li, Y.; Su, Y.; Wu, S.-T. Planar Alvarez tunable lens based on polymetric liquid crystal Pancharatnam-Berry optical elements. *Opt. Express* **2022**, *30*, 34655–34664. [CrossRef]
43. Mitov, M. Cholesteric liquid crystals with a broad light reflection band. *Adv. Mater.* **2012**, *24*, 6260–6276. [CrossRef]
44. Tamaoki, N. Cholesteric liquid crystals for color information technology. *Adv. Mater.* **2001**, *13*, 1135–1147. [CrossRef]
45. Zhang, W.; Froyen, A.A.; Schenning, A.P.; Zhou, G.; Debije, M.G.; de Haan, L.T. Temperature-responsive photonic devices based on cholesteric liquid crystals. *Adv. Photonics Res.* **2021**, *2*, 2100016. [CrossRef]
46. Love, G.D.; Hoffman, D.M.; Hands, P.J.; Gao, J.; Kirby, A.K.; Banks, M.S. High-speed switchable lens enables the development of a volumetric stereoscopic display. *Opt. Express* **2009**, *17*, 15716–15725. [CrossRef] [PubMed]
47. Gooch, C.; Tarry, H. The optical properties of twisted nematic liquid crystal structures with twist angles $\leq$ 90 degrees. *J. Phys. D Appl. Phys.* **1975**, *8*, 1575. [CrossRef]
48. Chao, A.; Huang, K.; Tsai, C.; Hung, Y.; Cheng, H.; Yeh, W.; Yu, C.; Wu, H. The Fastest Response TN-Type TFT LCD of the World Likes OCB Level. In *SID Symposium Digest of Technical Papers*; Wiley: Long Beach, CA, USA. 2007.

49. Lee, C.-K.; Moon, S.; Lee, S.; Yoo, D.; Hong, J.-Y.; Lee, B. Compact three-dimensional head-mounted display system with Savart plate. *Opt. Express* **2016**, *24*, 19531–19544. [CrossRef]
50. Takaki, Y. Development of super multi-view displays. *ITE Trans. Media Technol. Appl.* **2014**, *2*, 8–14.
51. Liu, L.; Pang, Z.; Teng, D. Super multi-view three-dimensional display technique for portable devices. *Opt. Express* **2016**, *24*, 4421–4430. [CrossRef]
52. Kajiki, Y.; Yoshikawa, H.; Honda, T. Hologramlike video images by 45-view stereoscopic display. In *Stereoscopic Displays and Virtual Reality Systems IV*; SPIE: San Jose, CA, USA, 1997.
53. Ueno, T.; Takaki, Y. Super multi-view near-eye display to solve vergence–accommodation conflict. *Opt. Express* **2018**, *26*, 30703–30715. [CrossRef]
54. Liu, L.; Ye, Q.; Pang, Z.; Huang, H.; Lai, C.; Teng, D. Polarization enlargement of FOV in Super Multi-view display based on near-eye timing-apertures. *Opt. Express* **2022**, *30*, 1841–1859. [CrossRef]
55. Wang, L.; Li, Y.; Liu, S.; Su, Y.; Teng, D. Large depth of range Maxwellian-viewing SMV near-eye display based on a Pancharatnam-Berry optical element. *IEEE Photonics J.* **2021**, *14*, 1–7. [CrossRef]
56. Tay, S.; Blanche, P.-A.; Voorakaranam, R.; Tunç, A.; Lin, W.; Rokutanda, S.; Gu, T.; Flores, D.; Wang, P.; Li, G. An updatable holographic three-dimensional display. *Nature* **2008**, *451*, 694–698. [CrossRef] [PubMed]
57. Wakunami, K.; Hsieh, P.-Y.; Oi, R.; Senoh, T.; Sasaki, H.; Ichihashi, Y.; Okui, M.; Huang, Y.-P.; Yamamoto, K. Projection-type see-through holographic three-dimensional display. *Nat. Commun.* **2016**, *7*, 12954. [CrossRef] [PubMed]
58. Kozacki, T.; Chlipala, M. Color holographic display with white light LED source and single phase only SLM. *Opt. Express* **2016**, *24*, 2189–2199. [CrossRef]
59. Lin, S.-F.; Wang, D.; Wang, Q.-H.; Kim, E.-S. Full-color holographic 3D display system using off-axis color-multiplexed-hologram on single SLM. *Opt. Lasers Eng.* **2020**, *126*, 105895. [CrossRef]
60. Li, X.; Chen, C.; Gao, H.; He, Z.; Xiong, Y.; Li, H.; Hu, W.; Ye, Z.; He, G.; Lu, J. Video-rate holographic display using azo-dye-doped liquid crystal. *J. Disp. Technol.* **2013**, *10*, 438–443. [CrossRef]
61. Li, X.; Chen, C.; Li, Y.; Zhou, P.; Jiang, X.; Rong, N.; Liu, S.; He, G.; Lu, J.; Su, Y. High-efficiency video-rate holographic display using quantum dot doped liquid crystal. *J. Disp. Technol.* **2016**, *12*, 362–367. [CrossRef]
62. Li, X.; Li, Y.; Xiang, Y.; Rong, N.; Zhou, P.; Liu, S.; Lu, J.; Su, Y. Highly photorefractive hybrid liquid crystal device for a video-rate holographic display. *Opt. Express* **2016**, *24*, 8824–8831. [CrossRef]
63. Patel, J.S.; Rastani, K. Electrically controlled polarization-independent liquid-crystal Fresnel lens arrays. *Opt. Lett.* **1991**, *16*, 532–534. [CrossRef]
64. Chang, Y.-C.; Jen, T.-H.; Ting, C.-H.; Huang, Y.-P. High-resistance liquid-crystal lens array for rotatable 2D/3D autostereoscopic display. *Opt. Express* **2014**, *22*, 2714–2724. [CrossRef]
65. Chu, F.; Wang, D.; Liu, C.; Li, L.; Wang, Q.-H. Multi-view 2D/3D switchable display with cylindrical liquid crystal lens array. *Crystals* **2021**, *11*, 715. [CrossRef]
66. Ren, H.; Fan, Y.-H.; Wu, S.-T. Liquid-crystal microlens arrays using patterned polymer networks. *Opt. Lett.* **2004**, *29*, 1608–1610. [CrossRef] [PubMed]
67. He, Z.; Lee, Y.-H.; Chen, R.; Chanda, D.; Wu, S.-T. Switchable Pancharatnam-Berry microlens array with nano-imprinted liquid crystal alignment. *Opt. Lett.* **2018**, *43*, 5062–5065. [CrossRef] [PubMed]
68. Chu, F.; Guo, Y.-Q.; Zhang, Y.-X.; Duan, W.; Zhang, H.-L.; Tian, L.-L.; Li, L.; Wang, Q.-H. Four-mode 2D/3D switchable display with a 1D/2D convertible liquid crystal lens array. *Opt. Express* **2021**, *29*, 37464–37475. [CrossRef] [PubMed]
69. Dou, H.; Chu, F.; Guo, Y.-Q.; Tian, L.-L.; Wang, Q.-H.; Sun, Y.-B. Large aperture liquid crystal lens array using a composited alignment layer. *Opt. Express* **2018**, *26*, 9254–9262. [CrossRef]
70. Li, R.; Zhang, H.-L.; Chu, F.; Wang, Q.-H. Compact integral imaging 2D/3D compatible display based on liquid crystal micro-lens array. *Liq. Cryst.* **2021**, *49*, 512–522. [CrossRef]
71. Hassanfiroozi, A.; Huang, Y.-P.; Javidi, B.; Shieh, H.-P.D. Hexagonal liquid crystal lens array for 3D endoscopy. *Opt. Express* **2015**, *23*, 971–981. [CrossRef]
72. Zhang, Y.; Weng, X.; Liu, P.; Wu, C.; Sun, L.; Yan, Q.; Zhou, X.; Guo, T. Electrically high-resistance liquid crystal micro-lens arrays with high performances for integral imaging 3D display. *Opt. Commun.* **2020**, *462*, 125299. [CrossRef]
73. Li, S.-Q.; Xu, X.; Maruthiyodan Veetil, R.; Valuckas, V.; Paniagua-Domínguez, R.; Kuznetsov, A.I. Phase-only transmissive spatial light modulator based on tunable dielectric metasurface. *Science* **2019**, *364*, 1087–1090. [CrossRef]
74. Luo, Z.; Li, Y.; Semmen, J.; Rao, Y.; Wu, S.-T. Achromatic diffractive liquid-crystal optics for virtual reality displays. *Light Sci. Appl.* **2023**, *12*, 230. [CrossRef]